Applied Mathematics & Information Sciences
An International Journal

Influence of heat and chemical reactions on blood flow through an anisotropically tapered elastic arteries with overlapping stenosis

Kh. S. Mekheimer[1], *M. H. Haroun*[2] *and M. A. El Kot*[3]

[1] Department of Mathematics, Faculty of Science, Al-Azhar University, Nasr city 11884, Cairo, Egypt
[2] Department of Mathematics, Faculty of Education, Ain Shams University, Cairo, Egypt
[3] Department of Mathematics, Faculty of Science, Suez Canal University, Suez, Egypt

Received: Jul 8, 2011; Revised Oct. 4, 2011; Accepted Nov. 26, 2011
Published online: 1 May 2012

Abstract: In the present investigation, we have studied the influence of heat and chemical reactions on blood flow through anisotropically tapered elastic artery with overlapping stenosis. The nature of blood in small arteries are analyzed mathematically by considering it as micropolar fluid. The analysis is carried out for an artery with a mild stenosis. Analytical expressions for the axial velocity, the stream function, the circumferential microrotation, the temperature distribution, the concentration of fluid, the resistance impedance and the wall shear stress distribution have been computed numerically and the results were studied for various values of the physical parameters, such as the the coupling number N, the micropolar parameter m, the taper angle ϕ, the maximum height of stenosis δ, the Soret number S_r, the Brickmann number B_r, the degree of anisotropy of the vessel wall n, the initial circumferential viscoelastic stress $T_{\theta o}$, the circumferential Poisson's ratio σ_θ and the contribution of the elastic constraints to the total tethering K. The obtained results for different values of parameters into the problem under consideration show that the magnitude of the axial velocity is higher for a Newtonian fluid than that for a micropolar fluid also the transmission of axial velocity curves through a free tube is substantially higher than that through the tethered tube. Further the temperature profile increase rapidly for small values of micropolar parameter (micropolar spin parameter) while the concentration profile has an opposite behavior. The trapping bolus increase in size as the coupling number increases (the particle size increases) while the volume of the bolus decreases by increasing of micropolar parameter (micropolar spin parameter). Finally the size of trapped bolus for the stream lines in the free isotropic tube is smaller than those in the tethered tube.

Keywords: Micropolar fluid, anisotropic artery, mild stenosis, the degree of anisotropy.

1. Introduction

Stenoses in the arteries of mammals are a common occurrence and for many years researchers have endeavored to model the flow of blood through stenosed arteries experimentally and theoretically. The deposition of cholesterol and proliferation of the connective tissues in the arterial wall form plaques which grow inward and restrict the blood flow. In order to have a fuller understanding of the development of these diseases, an accurate knowledge of the mechanical properties of the vascular wall together with the flow characteristics of blood are indispensable. Thus relevant information is deemed to be of great help in the treatment of vascular diseases and also to bioengineers who are engaged in the design and construction of improved artificial organs. Perhaps the actual cause of abnormal growth in an artery is not completely clear to the theoretical investigators but its effect over the cardiovascular system has been determined by studying the flow characteristics of blood in the stenosed area. Although the applicability of a purely mechanical model for such a physiological problem has obvious limitations, vascular rheology together with hemodynamic factors are predominant in the development and progression of arterial stenosis [1].

The theory of micropolar fluid due to Eringen [2] is a subclass of microfluids. In the micropolar theory a part from the classical velocity field, the microrotation vector and the gyration parameter are introduced to inves-

* Corresponding author: e-mail: kh_mekheimer@yahoo.com

tigate the kinematics of microrotations. The micropolar fluid, e.g., liquid crystals, suspensions and animal blood etc, consists of randomly oriented bar-like elements or dumb-bell molecules and each volume element has microrotation about its centroid, in addition to translatory motion in an average sense. The micropolar fluid theory deviates from the classical Navier-Stokes model of viscous fluid, regarding the suspenance of couple stress in the fluid and the non symmetry of the stress tensor. The micropolarity of the fluid was found to be prominent in tubes of small radius whereas in larger tubes it was hardly perceptible. The micropolar fluid is considered to the model of the blood flow in small arteries and the calculation of theoretical velocity profiles is observed in good agreement with experimental data.

Recently, the study of the effects of heat and chemical reactions on blood has become quite interesting to many researchers both from the theoretical and experimental point of view because the quantitative prediction of blood flow rate and heat generation are of great importance for diagnosing blood circulation illness and for the noninvasive measurement of blood glucose. An understanding of convection heat transfer in non-Newtonian fluids inside pipes is crucial to the design of several types of thermal equipment. From this viewpoint, heat transfer problems of this type have been investigated by a large number of researchers [3–10].

The important contributions of recent years to the topic are referenced in the literature [11–14]. Many of researches about arteriosclerotic development indicate that the studies are mainly concerned with the single symmetric and non-symmetric stenoses while the stenoses may develop in series (multiple stenoses) or may be of irregular shapes or overlapping or of composite in nature. Some studies considered an overlapping stenosis in the blood vessel segment. Chakravarty and Mandal [15] noted that the problem becomes more acute in the presence of an overlapping stenosis in the artery instead of a mild one. The effect of vessel tapering is another important factor that was considered. Chakravarty and Mandal [16] formulated the problem on tapered blood vessel segment having an overlapping stenosis. Ismail et al. [17] study the power-law model of blood flow through an overlapping stenosed artery where an improved shape of the time-variant stenosis in the tapered arterial lumen is given and the vascular wall deformability is taken to be elastic (moving wall). Recently, Mekheimer et. al. [18] study the effect of induced magnetic field on blood flow through an anisotropically tapered elastic arteries with overlapping stenosis in an annulus.

Many recent researches have studied the effect of heat and mass transfer on the flow of blood but in all of these studies the effect of motion of the arterial wall when it is subjected to inertial forces, surface forces and the forces of constraint representing the reactions of the surrounding connective tissues have been neglected. In this paper, we interest with studying the effect of elastic wall properties on the flow of micropolar fluid (as a blood model) through an artery with overlapping stenosis. The problem is first modeled and the non-dimensional governing equations are formulated. The non-dimensional governing equations in the case of mild stenosis and the corresponding boundary conditions are prescribed then solved analytically for the axial velocity and the circumferential microrotation, the temperature distribution and the concentration of fluid. The obtained results have been discussed for various values of the problem parameters. Also the contour plots for the stream function are discussed. Finally, the main finding of the results are summarized as a concluding remarks.

2. Formulation of the problem

Consider an incompressible micropolar fluid of viscosity μ and density ρ flowing through a tube of finite length L with overlapping stenosis. The tube material is being treated as anisotropic linear viscoelastic. Let (r, θ, z) be the coordinates of a material point in the cylindrical polar coordinate system where z- axis is taken along the axis of the artery while r, θ are along the radial and circumferential directions respectively. Further, we assume that $r = 0$ is taken as the axis of the symmetry of the tube. The heat and mass transfer phenomenons is taken into account by giving temperature T_1 and concentration C_1 to the wall of the tube, while at the center of the tube we are considering symmetry condition on both temperature and concentration. The geometry of the elastic (moving wall) arterial wall of the time-variant overlapping stenosis for different taper angles (see Fig. 1) is written mathematically as [17]

$$\begin{aligned} R(z,t) = [(mz + R_o) - \frac{\delta \cos\phi}{L_o}(z-d)\{11 - \frac{94}{3L_o}(z-d) \\ + \frac{32}{L_o^2}(z-d)^2 - \frac{32}{3L_o^3}(z-d)^3\}]\Omega(t), \\ d \le z \le d + \frac{3L_o}{2} \\ = (mz + R_o)\Omega(t) \qquad \text{otherwise} \end{aligned} \tag{1}$$

where $R(z,t)$ denotes the radius of the tapered arterial segment in the constricted region, R_o is the constant radius of the normal artery in the non-stenotic region, ϕ is the angle of tapering, $\frac{3L_o}{2}$ is the length of overlapping stenosis, d is the location of the stenosis, $\delta \cos\phi$ is taken to be the critical height of the overlapping stenosis and $m = (\tan\phi)$ represents the slope of the tapered vessel. We can explore the possibility of different shapes of the artery viz, the converging tapering ($\phi < 0$), non-tapered artery ($\phi = 0$) and the diverging tapering ($\phi > 0$)[19]. The time-variant parameter $\Omega(t)$ is taken to be

$$\Omega(t) = 1 - b(\cos\omega t - 1)\exp[-b\omega t], \tag{2}$$

where b is a constant, ω represents the angular frequency of the forced oscillation and t is the time.

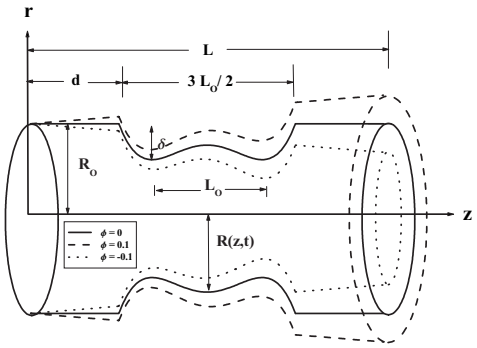

Figure 1 Schematic diagram of overlapping stenosed artery.

The equations governing for unsteady flow of an incompressible micropolar fluid in the absence of body force and body couple are

$$\nabla.V = 0, \tag{3}$$

$$\rho(\frac{\partial V}{\partial t} + V.\nabla V) = -\nabla p + k\nabla \times V + (\mu + k)\nabla^2 V, \tag{4}$$

$$\rho j(\frac{\partial w}{\partial t} + V.\nabla w) = -2kw + k\nabla \times V - \gamma(\nabla \times \nabla \times w) + (\alpha + \beta + \gamma)\nabla(\nabla.w), \tag{5}$$

where p is the fluid pressure, μ and k are the coefficients of shear and vortex viscosities, α, β and γ are the respective coefficients of viscosities, V is the velocity vector, w is the microrotation vector and j is the microgyration parameter. Further, the material constants μ, k, α, β and γ satisfy the following inequalities [20]

$$2\mu + k \geq 0, \quad k \geq 0, \quad 3\alpha + \beta + \gamma \geq 0, \quad \gamma \geq |\beta|. \tag{6}$$

The energy equation is defined as follow

$$\rho c_p(\frac{\partial T}{\partial t} + V.\nabla T) = \Phi + F\nabla^2 T, \tag{7}$$

and Φ is the frictional heating can be written by

$$\Phi = 2\mu[(\frac{\partial V_r}{\partial r})^2 + \frac{1}{2}(\frac{\partial V_r}{\partial z} + \frac{\partial V_z}{\partial r})^2 + (\frac{\partial V_z}{\partial z})^2]. \tag{8}$$

It should be mentioned that the mass concentration equation can be found in the book by Bejan [21] in the form

$$(\frac{\partial C}{\partial t} + V.\nabla C) = D\nabla^2 C + \frac{DF_T}{T_m}\nabla^2 T, \tag{9}$$

where V_r and V_z are the velocity components in r and z directions respectively, T is the temperature, C is the concentration of fluid, F denotes the thermal conductivity, c_p is the specific heat at constant pressure, T_m is the temperature of the medium, D is the coefficients of mass diffusivity and F_T is the thermal-diffusion ratio.

The governing equations of motion for the arterial wall when it is subjected to inertial forces, surface forces and the forces of constraint representing the reactions of the surrounding connective tissues, are given by [1,22–24]

$$M_o\frac{\partial^2 \xi}{\partial t^2} + C_l\frac{\partial \xi}{\partial t} + K_l\xi = -\mu(\frac{\partial V_z}{\partial r} + \frac{\partial V_r}{\partial z})|_{r=R_o} + \frac{\partial \eta}{\partial z}(\frac{T_{to} - T_{\theta o}}{R_o}) + \frac{E_t h}{1 - \sigma_\theta \sigma_t}(\frac{\sigma_\theta}{R_o}\frac{\partial \eta}{\partial z} + \frac{\partial^2 \xi}{\partial z^2}) \tag{10}$$

$$M_o\frac{\partial^2 \eta}{\partial t^2} + C_r\frac{\partial \eta}{\partial t} + K_r\eta = (p - 2\mu\frac{\partial V_r}{\partial r})|_{r=R_o} + \frac{\eta}{a^2}T_{\theta o} + T_{to}\frac{\partial^2 \eta}{\partial z^2} - \frac{E_\theta h}{R_o(1 - \sigma_\theta\sigma_t)}(\frac{\eta}{R_o} + \sigma_t\frac{\partial \xi}{\partial z}), \tag{11}$$

in which $M_o = \rho_o h + M_a$ where ρ_o and h are the mass density and thickness of the arterial wall respectively. (ξ, η) represent the displacement components of the vessel wall along the axial and radial directions respectively while $(T_{to}, T_{\theta o})$ are the initial respective viscoelastic stress components acting along the longitudinal and the circumferential directions. K_l, C_l and M_a represent (per unit area) the spring coefficient, the frictional coefficient of the dashpot and the additional mass of the mechanical model respectively in the longitudinal tethering and K_r, C_r are those in the radial direction. E_θ and E_t are Young's moduli in the circumferential and longitudinal directions, respectively, σ_θ and σ_t are the corresponding Poisson's ratios.

The boundary conditions are:

$$V_r = 0, \quad \frac{\partial V_z}{\partial r} = 0, \quad \frac{\partial T}{\partial r} = 0, \quad \frac{\partial C}{\partial r} = 0, \quad V_z \quad \text{and} \quad \nu_\theta \quad \text{are finite at} \quad r = 0, \tag{12}$$

$$V_r = \frac{\partial \eta}{\partial t}, \quad V_z = \frac{\partial \xi}{\partial t}, \quad \nu_\theta = 0 \quad [25],$$
$$T = T_1, \quad C = C_1 \quad \text{on} \quad r = R(z,t). \tag{13}$$

Since the flow is axisymmetric, all the variables are independent of θ. Hence, for this flow let the velocity vector is given by $V = (V_r, 0, V_z)$ and the microrotation vector $w = (0, \nu_\theta, 0)$. We introduce the following non-dimensional variables:

$$r = R_o r', \quad z = L_o z', \quad \omega = \frac{c}{L_o}\omega', \quad \xi = L_o\xi',$$
$$\eta = L_o\eta', \quad V_r = \frac{\delta c}{L_o}V_r', \quad V_z = cV_z', \quad R = R_o R',$$
$$t = \frac{L_o}{c}t', \quad p = \frac{cL_o\mu}{R_o^2}p', \quad j = R_0^2 j', \quad \nu_\theta = \frac{c}{R_0}\nu_\theta',$$
$$M_o = \rho R_o M_o', \quad C_l = \rho c C_l', \quad C_r = \rho c C_r', \quad h = R_o h',$$
$$K_l = \frac{\rho c^2}{R_o}K_l', \quad K_r = \frac{\rho c^2}{R_o}K_r', \quad T_{to} = \rho c^2 R_o T_{to}',$$
$$T_{\theta o} = \rho c^2 R_o T_{\theta o}', \quad E_t = \rho c^2 E_t', \quad E_\theta = \rho c^2 E_\theta',$$
$$T = T_1 + (T_o - T_1)\Theta, \quad C = C_1 + (C_o - C_1)\Sigma, \tag{14}$$

where c is the velocity averaged over the section of the tube with radius R_o.

To proceed, we non-dimensionalize Eqs. (3-5) and (7-11) by using Eq. **(??)**, the non-dimensional governing equations after dropping the dashes can be written as:

$$\delta^*(\frac{\partial V_r}{\partial r}+\frac{V_r}{r})+\frac{\partial V_z}{\partial z}=0, \tag{15}$$

$$R_e\delta^*\varepsilon^3(\frac{\partial V_r}{\partial t}+\delta^* V_r\frac{\partial V_r}{\partial r}+V_z\frac{\partial V_r}{\partial z})=-\frac{\partial p}{\partial r}+\frac{\varepsilon^2}{1-N}$$
$$(-N\frac{\partial v_\theta}{\partial z}+\delta^*(\frac{\partial^2 V_r}{\partial r^2}+\frac{1}{r}\frac{\partial V_r}{\partial r}-\frac{V_r}{r^2}+\varepsilon^2\frac{\partial^2 V_r}{\partial z^2})), \tag{16}$$

$$R_e\varepsilon(\frac{\partial V_z}{\partial t}+\delta^* V_r\frac{\partial V_z}{\partial r}+V_z\frac{\partial V_z}{\partial z})=-\frac{\partial p}{\partial z}+\frac{1}{1-N}$$
$$(\frac{N}{r}\frac{\partial(r\nu_\theta)}{\partial r}+\frac{\partial^2 V_z}{\partial r^2}+\frac{1}{r}\frac{\partial V_z}{\partial r}+\varepsilon^2\frac{\partial^2 V_z}{\partial z^2}), \tag{17}$$

$$\frac{jR_e\varepsilon(1-N)}{N}(\frac{\partial \nu_\theta}{\partial t}+\delta^* V_r\frac{\partial \nu_\theta}{\partial r}+V_z\frac{\partial \nu_\theta}{\partial z})=$$
$$-2\nu_\theta+(\delta^*\varepsilon^2\frac{\partial V_r}{\partial z}-\frac{\partial V_z}{\partial r})+\frac{2-N}{m^2}$$
$$[\frac{\partial}{\partial r}(\frac{1}{r}\frac{\partial(r\nu_\theta)}{\partial r})+\varepsilon^2\frac{\partial^2 \nu_\theta}{\partial z^2}], \tag{18}$$

$$\varepsilon^2 M_o\frac{\partial^2\xi}{\partial t^2}+\varepsilon C_l\frac{\partial \xi}{\partial t}+K_l\xi=$$
$$-\frac{\varepsilon}{R_e}(\frac{\partial V_z}{\partial r}+\delta^*\varepsilon^2\frac{\partial V_r}{\partial z})|_{r=1}+\varepsilon\frac{\partial \eta}{\partial z}(T_{to}-T_{\theta o})$$
$$+\varepsilon\frac{E_t h}{1-\sigma_\theta\sigma_t}(\sigma_\theta\frac{\partial \eta}{\partial z}+\varepsilon\frac{\partial^2\xi}{\partial z^2}), \tag{19}$$

$$\varepsilon^2 M_o\frac{\partial^2\eta}{\partial t^2}+\varepsilon C_r\frac{\partial \eta}{\partial t}+K_r\eta=$$
$$\frac{1}{R_e}(p-2\delta^*\varepsilon^2\frac{\partial V_r}{\partial r})|_{r=1}+T_{\theta o}\eta+\varepsilon^2 T_{to}\frac{\partial^2\eta}{\partial z^2}$$
$$-\frac{E_\theta h}{1-\sigma_\theta\sigma_t}(\eta+\varepsilon\sigma_t\frac{\partial\xi}{\partial z}), \tag{20}$$

$$R_e\varepsilon(\frac{\partial \Theta}{\partial t}+\delta^* V_r\frac{\partial \Theta}{\partial r}+V_z\frac{\partial \Theta}{\partial z})=2E_c(\varepsilon^2\delta^{*2}(\frac{\partial V_r}{\partial r})^2$$
$$+\frac{1}{2}(\varepsilon^2\delta^*\frac{\partial V_r}{\partial z}+\frac{\partial V_z}{\partial r})^2+\varepsilon^2(\frac{\partial V_z}{\partial z})^2)$$
$$+\frac{1}{P_r}(\frac{\partial^2\Theta}{\partial r^2}+\frac{1}{r}\frac{\partial\Theta}{\partial r}+\varepsilon^2\frac{\partial^2\Theta}{\partial z^2}), \tag{21}$$

$$R_e\varepsilon(\frac{\partial \Sigma}{\partial t}+\delta^* V_r\frac{\partial \Sigma}{\partial r}+V_z\frac{\partial \Sigma}{\partial z})=$$
$$\frac{1}{S_c}(\frac{\partial^2\Sigma}{\partial r^2}+\frac{1}{r}\frac{\partial\Sigma}{\partial r}+\varepsilon^2\frac{\partial^2\Sigma}{\partial z^2})$$
$$+S_r(\frac{\partial^2\Theta}{\partial r^2}+\frac{1}{r}\frac{\partial\Theta}{\partial r}+\varepsilon^2\frac{\partial^2\Theta}{\partial z^2}). \tag{22}$$

The appropriate equations describing the flow of micrpolar fluid in the case of a mild stenosis ($\delta^*=\frac{\delta}{R_o}<<1$), subject to the additional condition ($\varepsilon=\frac{R_o}{L_o}\simeq o(1)$) [26] can be written as:

$$\frac{\partial p}{\partial r}=0, \tag{23}$$

$$\frac{\partial p}{\partial z}=\frac{1}{1-N}(\frac{1}{r}\frac{\partial}{\partial r}(r\frac{\partial V_z}{\partial r})+\frac{N}{r}\frac{\partial(\nu_\theta)}{\partial r}), \tag{24}$$

$$2v_\theta=-\frac{\partial V_z}{\partial r}+\frac{2-N}{m^2}\frac{\partial}{\partial r}(\frac{1}{r}\frac{\partial(r\nu_\theta)}{\partial r}), \tag{25}$$

$$K_l\xi=0 \tag{26}$$

$$p(z,t)=R_e(K_r+\frac{E_\theta h}{1-n\sigma_\theta^2}-T_{\theta o})\eta(z,t) \tag{27}$$

$$\frac{1}{r}\frac{\partial}{\partial r}(r\frac{\partial\Theta}{\partial r})+B_r(\frac{\partial V_z}{\partial r})^2=0, \tag{28}$$

$$\frac{\partial}{\partial r}(r\frac{\partial\Sigma}{\partial r})+S_rS_c\frac{\partial}{\partial r}(r\frac{\partial\Theta}{\partial r})=0, \tag{29}$$

where $N=\frac{k}{(\mu+k)}$ is the coupling number ($0\le N\prec 1$) [20] and $m^2=\frac{R_o^2k(\mu+k)}{\gamma(\mu+k)}$ is the micropolar parameter, $R_e=\frac{\rho cR_o}{\mu}$ is suction Reynolds number, $P_r=\frac{c_p\mu}{F}$ is the Prandtl number of the fluid, $E_c=\frac{c^2}{c_p(T_o-T_1)}$ and $S_c=\frac{\mu}{D\rho}$ are the dimensionless quantities, $S_r=\frac{\rho DF_T(T_o-T_1)}{\mu T_m(C_o-C_1)}$ is Soret number, $B_r=E_cP_r$ is Brickmann number and $n=\frac{\sigma_t}{\sigma_\theta}$ is the degree of anisotropy of the vessel wall

The corresponding boundary conditions (dropping dashes):

$$\frac{\partial V_z}{\partial r}=0,\quad \frac{\partial\Theta}{\partial r}=0,\quad \frac{\partial\Sigma}{\partial r}=0,\quad \text{on}\quad r=0, \tag{30}$$

$$(\frac{\delta}{L_o})V_r=\frac{\partial\eta}{\partial t},V_z=\frac{\partial\xi}{\partial t},\Theta=\Sigma=0\quad\text{on}\quad r=R, \tag{31}$$

where

$$R(z,t)=[(m^*z+1)-\delta\cos\phi(z-d^*)\{11-\frac{94}{3}(z-d^*)$$
$$+32(z-d^*)^2-\frac{32}{3}(z-d^*)^3\}]\Omega(t),$$
$$d^*\le z\le d^*+\frac{3}{2}$$
$$=(m^*z+1)\Omega(t)\qquad\text{otherwise} \tag{32}$$

where $m^*=L_om$ and $d^*=\frac{d}{L_o}$.

3. Solution of the problem

By using the Eq. (26) and the boundary condition (31), we can note that $\xi=0$ where $K_l\neq 0$ and for ($\frac{\delta}{L_o}<<1$), we assume that the radial motion for arterial wall decreases with increasing z and can be written in the form $\eta(z)=\exp[-kz]$ [[1], [24], [27]] where η independent on the time and k represents the wave number of the harmonic

oscillation. Noting the fact p is a function of z only from Eq. (23), the fluid pressure can be written as

$$p(z) = R_e(K_r + \frac{E_\theta h}{1 - n\sigma_\theta^2} - T_{\theta o})\exp[-kz]. \quad (33)$$

And Eq. (24) can be rewritten in the form

$$\frac{\partial}{\partial r}\{r\frac{\partial V_z}{\partial r} + Nr\nu_\theta - (1-N)\frac{r^2}{2}\frac{\partial p}{\partial z}\} = 0, \quad (34)$$

hence, we get

$$\frac{\partial V_z}{\partial r} = (1-N)\{\frac{r}{2}\frac{\partial p}{\partial z} + \frac{A_1}{r}\} - N\nu_\theta. \quad (35)$$

Using Eq. (35) in Eq. (25) we get

$$\frac{\partial^2 \nu_\theta}{\partial r^2} + \frac{1}{r}\frac{\partial \nu_\theta}{\partial r} - (m^2 + \frac{1}{r^2})\nu_\theta = \frac{(1-N)m^2}{(2-N)}\{\frac{r}{2}\frac{\partial p}{\partial x} + \frac{A_1}{r}\}, \quad (36)$$

and its general solution is

$$\nu_\theta = A_2 I_1(mr) + A_2 K_1(mr) - \frac{1-N}{2-N}\{\frac{r}{2}\frac{\partial p}{\partial x} + \frac{A_1}{r}\}, \quad (37)$$

where $I_1(mr)$ and $K_1(mr)$ are modified Bessel functions of first order, first and second kind respectively. Substituting Eq. (37) into Eq. (35) and integrating we obtain

$$V_z = (\frac{1-N}{2-N})\{\frac{r^2}{2}\frac{\partial p}{\partial x} + A_1\log(r)\} + \frac{N}{m}\{-A_2 I_0(mr) + A_3 K_0(mr)\} + A_4, \quad (38)$$

where $A_1(z), A_2(z), A_3(z)$ and $A_4(z)$ are the constants of integration, $I_o(mr)$ and $K_o(mr)$ are modified Bessel functions of zeroth - order and by using the boundary conditions, we can get the axial velocity and the circumferential microrotation in the form

$$V_z(r,z,t) = \frac{1-N}{2(2-N)}\frac{dp}{dz}(r^2 - R^2 + \frac{NR}{m}(\frac{I_0(mR) - I_0(mr)}{I_1(mR)})), \quad (39)$$

$$\nu_\theta(r,z,t) = \frac{1-N}{2(2-N)}\frac{dp}{dz}(\frac{RI_1(mr)}{I_1(mR)} - r), \quad (40)$$

To find the general solution of the temperature, we Substitute Eq. (39) into Eq. (28) and integrating we get

$$\Theta = -B_r\Xi^2[\frac{r^4}{4} - \frac{4\Pi}{m^3}(mrI_1(mr) + 2(1 - I_o(mr)) + \frac{\Pi^2}{2m^2}((1-m^2r^2)I_o^2(mr) + mrI_o(mr)I_1(mr) + m^2r^2I_1^2(mr) - 1)] + A_5\ln(r) + A_6, \quad (41)$$

where A_5 and A_6 are the constants of integration, $I_o(x)$ and $I_1(x)$ are the modified Bessel functions of zeroth and first order respectively, $\Xi = \frac{(1-N)}{2(2-N)}(\frac{dp}{dz})$ and $\Pi = \frac{NR}{I_1(mR)}$.

By using the boundary conditions, we can get the temperature as

$$\Theta(r,z,t) = -B_r\Xi^2[\frac{r^4 - R^4}{4} - \frac{4\Pi}{m^3}(m(rI_1(mr) - RI_1(mR)) + 2(I_o(mR) - I_o(mr))) + \frac{\Pi^2}{2m^2}((1-m^2r^2)I_o^2(mr) - (1-m^2R^2)I_o^2(mR) + m^2(r^2I_1^2(mr) - R^2I_1^2(mR)) + m(rI_o(mr)I_1(mr) - RI_o(mR)I_1(mR)))]. \quad (42)$$

Using Eqs. (42) and (29), we can find the solution of the concentration of fluid together with the corresponding boundary conditions in the form

$$\Sigma(r,z,t) = -S_rS_cB_r\Xi^2[\frac{r^4 - R^4}{4} - \frac{4\Pi}{m^3}(m(rI_1(mr) - RI_1(mR)) + 2(I_o(mR) - I_o(mr))) + \frac{\Pi^2}{2m^2}((1-m^2r^2)I_o^2(mr) - (1-m^2R^2)I_o^2(mR) + m^2(r^2I_1^2(mr) - R^2I_1^2(mR)) + m(rI_o(mr)I_1(mr) - RI_o(mR)I_1(mR)))]. \quad (43)$$

The corresponding stream function ($V_z = \frac{1}{r}\frac{\partial \psi}{\partial r}$ with $\psi = 0$ at $r = 0$) is

$$\psi(r,z,t) = \frac{1-N}{2(2-N)}\frac{dp}{dz}[\frac{r^4}{4} - \frac{R^2r^2}{2} + \frac{NR}{mI_1(mR)}(\frac{r^2I_0(mR)}{2} - \frac{rI_1(mr)}{m})]. \quad (44)$$

We can find the flux through the tube Q by

$$Q = 2\pi\int_0^R rV_z dr = (-\frac{\partial p}{\partial z})\frac{1}{F(z)}, \quad (45)$$

where

$$F(z) = \frac{(2-N)mI_1(mR)}{R^3(1-N)(RmI_1(mR) - 2NI_2(mR))}. \quad (46)$$

Since Q is constant for all the sections of the tube. The pressure drop across the length of the overlapping stenosis is

$$\Delta p = \int_0^{L^*}(-\frac{\partial p}{\partial z})dz = Q\int_0^{L^*}F(z)dz. \quad (47)$$

The resistance to flow (resistance impedance) experienced by the flowing blood in the arterial segment under consideration using Eq. (47) may be defined as

$$\lambda = \frac{\Delta p}{Q} = [\int_0^{d^*}I(z)dz + \int_{d^*}^{d^*+\frac{3}{2}}F(z)dz + \int_{d^*+\frac{3}{2}}^{L^*}I(z)dz], \quad (48)$$

where $L^* = \frac{L}{L_o}$ and $I(z) = F(z)|_{R=(m^*z+1)\Omega(t)}$.

It is very interesting to note for fluid in microcontinum (couple stress fluids, micropolar fluids, polar fluids, dipolar fluids, etc) the stress tensor is not symmetric. The nonzero

dimensionaless shear stresses in our problem are given by [20]

$$\tau_{zr} = \frac{\partial V_z}{\partial r} - \frac{N}{(1-N)}\nu_\theta, \tag{49}$$

$$\tau_{rz} = \frac{-1}{(1-N)}(\frac{\partial V_z}{\partial r} + N\nu_\theta). \tag{50}$$

From Eq. (50) we can find the expression for the wall shear stress by

$$\tau_{rz} = \frac{-1}{(1-N)}\frac{\partial V_z}{\partial r}|_{r=R}, \tag{51}$$

where $\nu_\theta = 0$ at $r = R$, by using Eqs. (39) and (45) we can find

$$\frac{\partial V_z}{\partial r}|_{r=R} = \frac{-1}{2}(1-N)\frac{\partial p}{\partial z}R(z) = 4QR(z)F(z). \tag{52}$$

The final expressions for the dimensionless resistance to flow $\bar{\lambda} = \frac{\lambda}{\lambda_0}$ and the wall shear stress $\bar{\tau}_{rz} = \frac{\tau_{rz}}{\tau_0}$ (dropping bars)

$$\lambda = \frac{1}{L^*}[\int_0^{d^*} I(z)dz + \int_{d^*}^{d^*+\frac{3}{2}} F(z)dz + \int_{d^*\frac{3}{2}}^{L^*} I(z)dz], \tag{53}$$

$$\tau_{rz} = \frac{(2-N)mI_1(mR)}{R^2(1-N)(RmI_1(mR) - 2NI_2(mR))}, \tag{54}$$

where $\lambda_0 = L^*$, $\tau_0 = Q$ and λ_0, τ_0 are the resistance to flow and the wall shear stress for a flow in a normal artery (no stenosis).

4. Discussion of the results

Computer codes are developed to evaluate the analytic results obtained for the axial velocity V_z, the circumferential microrotation ν_θ, the temperature distribution Θ, the concentration of fluid Σ, the resistance impedance λ and the wall shear stress distribution τ_{rz}. In order to observe the quantitative effects of the coupling parameter N, the micropolar parameter m, the taper angle ϕ, the maximum height of stenosis δ, the Soret number S_r, the Brickmann number B_r, the degree of anisotropy of the vessel wall n, the initial circumferential viscoelastic stress $T_{\theta o}$, the circumferential Poisson's ratio σ_θ and the contribution of the elastic constraints to the total tethering K. For the purpose of computational work, we use the following experimental data [[1] ,[23] ,[28]]

$$\mathrm{R}_e = 1, \quad b = 0.1, \quad L_o = 1\,, \quad d^* = 0.75\,, \quad k = 0.0021,$$

$$\omega = 7.854, \quad T_{\theta o} = 0.1, 10^4, 2x10^4, \quad \sigma_\theta = 0.5, 0.4, 0.3,$$

$$\mathrm{E}_\theta = 4x10^6\,, \quad h = 0.01, \quad K_r = R_eK = 10^4, 1.6x10^4.$$

The influence of the parameter which represent initial viscoelastic stress component acting along the circumferential direction $T_{\theta o}$ on propagation properties was previously analyzed by Atabek and Lew [24]. The effect of the Poisson's ratio in the circumferential direction σ_θ and the effect of the contribution of the elastic constraints to the total tethering K were investigated by Womersley [28].

The structure of the artery is quite complex and the tissue that constitutes artery walls consists of four major components are: (a) **Smooth muscle cells** (SMCs) represent the living component of the wall, where under the neural control they actively contract and expand thus changing the geometry and elastic modulus of the tissue. (b) **Elastin** is a rubber-like protein (scleroprotein) synthesized by the SMCs. It is present in artery walls in polymerized form, constituting the fenestrated network of thin fibers and can sustain large stresses and strains. (c) **Collagen** is also a protein synthesized by SMCs and it has the appearance of nylon where there are several types of collagen of which most common represent (66 percent in artery walls). (d) **Ground Substance** is a viscous substance like gel that embeds (scleroprotein) and (SMCs), so it is usually considered not to contribute to elastic properties of the wall. Many studies point out the arteries can be considered a focus for some diseases such as atherosclerosis (stenosis) or aneurysms because of the complex structure of the artery. The degree of anisotropy of the vessel wall n that responsible for the artery wall material depends on the material direction. The easiest way of understanding this fact is the presence of fibres (collagen, elastine and smooth muscle cells (SMCs)) in the wall such that the behavior in the direction of the fibres will be different than the transverse directions to the fibres. In the other hand if the fibres directions coincide with axial, circumferential and radial directions of the artery, the arterial wall material called orthotropic [30]. We take the data that represents a free isotropic tube as:

$$T_{\theta o} = 0, \qquad \sigma_\theta = 0.5, \qquad n = 1, \qquad K = 0, \tag{55}$$

where in the case of an isotropic tube $\sigma_\theta = \frac{1}{2}$, $n = 1$ and the tube is initially unstressed [31].

The effect of vessel tapering together with the shape of stenosis on the blood flow characteristics seem to be equally important and hence deserve special attention. The tapering is a significant aspect of mammalian arterial system. Thus, in this paper, we are interested in the flow through a tapered artery with stenosis. In an actual situation, the arterial wall thickness has not uniform shape, so we show the influences of the diverging , converging and nontapering arterial on the resistance to flow (resistance impedance) and the wall shear stress. The analysis of blood flow through tapered tubes is very important in understanding the behaviour of the flow as the taper of the tube is an important factor in the pressure development. It has been pointed out that the blood vessels bifurcate at frequent intervals and although the individual segments of arteries may be treated as uniform between bifurcations, the diameter of the artery decreases quite fast at each bifurcation [32]. It has been ob-

served that even for the small angles of taper (up to 2^o), the effects of tapering of the blood vessels cannot be neglected [33]. As pointed out by How and Black [34], this study is also very useful for the design of prosthetic blood vessels as the use of grafts of tapered lumen has the advantage of surgical benefits, the blood vessels being wider upstream.

Figs. (2-4) indicate how the axial velocity V_z is influenced by the unsteady behavior of the flowing blood as well as by the coupling parameter N, the micropolar parameter m, the degree of anisotropy of the vessel wall n, the initial circumferential viscoelastic stress $T_{\theta o}$, the circumferential Poisson's ratio σ_θ and the contribution of the elastic constraints to the total tethering K. Fig. (2) indicate that the magnitude of the axial velocity V_z decreases as the coupling parameter N increases (the particle size increases) while it increases as m increases (micropolar spin parameter increases) and the value of axial velocity is higher for a Newtonian fluid than that for a micropolar fluid. In Figs. (3) and (4) we use the data that represents a free tube as $(T_{\theta o} = 0, \sigma_\theta = 0.5, n = 1, K = 0)$. Fig. (3) indicate that the magnitude of the axial velocity V_z increases as the degree of anisotropy of the vessel wall n and the contribution of the elastic constraints to the total tethering K increases. Fig. (4) show that the magnitude of the axial velocity V_z increases as the circumferential Poisson's ratio σ_θ increases while it decreases by increasing the initial circumferential viscoelastic stress $T_{\theta o}$. Under stenotic conditions, the curves through the converging tapered artery $\phi = -0.1\ (< 0)$ are less than those in the non-tapered artery $\phi = 0$ and the diverging tapered artery $\phi = 0.1\ (> 0)$ (see Figs. (2-4)).

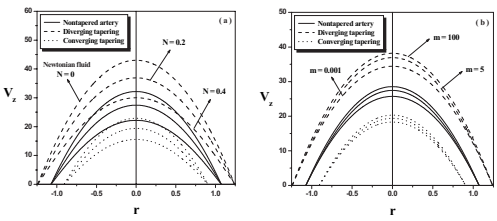

Figure 2 Variation of velocity profiles V_z for N and m at t = 0.5, z = 1.5, δ = 0.05, n = 1, K = 10^4, σ_θ = 0.5, $T_{\theta o}$ = 0.1 (panels (a) and (b) respectively).

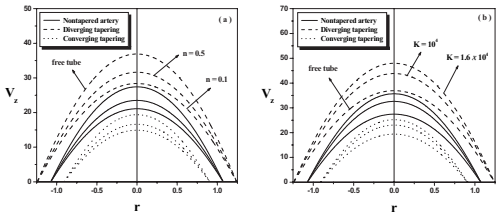

Figure 3 Variation of velocity profiles V_z for n and K at t = 0.5, z = 1.5, δ = 0.05, N = 0.2, m = 5 (panels (a) and (b) respectively).

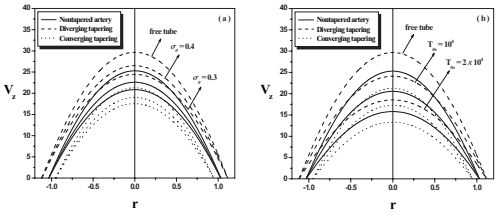

Figure 4 Variation of velocity profiles V_z for σ_θ and $T_{\theta o}$ at t = 0.5, z = 1.5, δ = 0.1, N = 0.2, m = 5 (panels (a) and (b) respectively).

Figs. (5-7) describe the distribution of the circumferential microrotation ν_θ with r for different values of N, m, n, K, σ_θ and $T_{\theta o}$. Fig. (5) indicate that the magnitude of the circumferential microrotation ν_θ decreases as the coupling number N increases while it increases as the micropolar parameter m increases. In Figs. (6) and (7) we use the data that represents a free tube as $(T_{\theta o} = 0, \sigma_\theta = 0.5, n = 1, K = 0)$. Fig. (6) indicate that the magnitude of the circumferential microrotation ν_θ increases as the degree of anisotropy of the vessel wall n and the contribution of the elastic constraints to the total tethering K increases. Also Fig. (7) explain that the magnitude of the circumferential microrotation ν_θ increases as the circumferential Poisson's ratio σ_θ increases while it decreases by increasing the initial circumferential viscoelastic stress $T_{\theta o}$. Further in the half region of the tube, the circumferential microrotation is one direction and in the other half it is in the opposite direction and it is zero at $r = 0$ (see Figs. (5-7)).

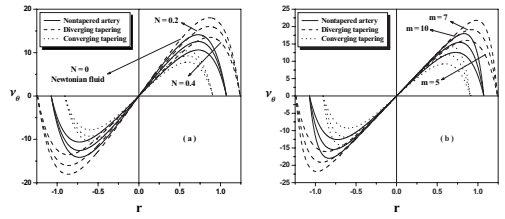

Figure 5 Variation of microrotation profiles ν_θ for N and m at t = 0.5, z = 1.5, δ = 0.05, n = 1, K = 10^4, σ_θ = 0.5, $T_{\theta o}$ = 0.1 (panels (a) and (b) respectively).

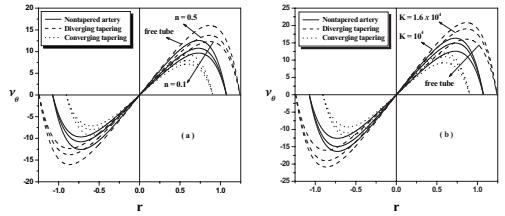

Figure 6 Variation of microrotation profiles ν_θ for n and K at t = 0.5, z = 1.5, δ = 0.05, N = 0.2, m = 5 (panels (a) and (b) respectively).

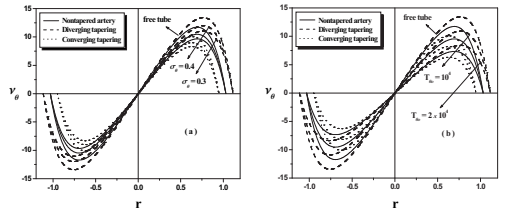

Figure 7 Variation of microrotation profiles ν_θ for σ_θ and $T_{\theta o}$ at t = 0.5, z = 1.5, δ = 0.05, N = 0.2, m = 5 (panels (a) and (b) respectively).

The variation of temperature profile for different values of the coupling parameter N, the degree of anisotropy of the vessel wall n, the contribution of the elastic constraints to the total tethering K, the circumferential Poisson's ratio σ_θ, the initial circumferential viscoelastic stress $T_{\theta o}$ and Brickmann number B_r is shown in Figs. (8-10). It is observed that with an increase in the degree of anisotropy of the vessel wall n, the contributions of the elastic constraints to the total tethering K, the circumferential Poisson's ratio σ_θ and Brickmann number B_r, temperature profile increases while it decreases with an increase in coupling parameter N and the initial circumferential viscoelastic stress $T_{\theta o}$. Also the curves through the converging tapered artery $\phi = -0.1$ (< 0) are less than those in the non-tapered artery $\phi = 0$ and the diverging tapered artery $\phi = 0.1$ (> 0). Moreover, the value of temperature profile is higher for a Newtonian fluid than that for a micropolar fluid. Fig. (11-a) is prepared to see the variation of temperature profile with micopolar parameter m for different values of taper angle ϕ. It is interesting to record that the temperature increases rapidly for small values of micropolar parameter m and then take a constant value as m increases. It is clear that the temperature distribution profile with the time t have a periodic oscillation form and there are three time cycles where the length of the cycle is equal to 1.6 approximately (see Fig. (11-b)). In the first cycle, the magnitude of the temperature distribution starts increasing to reach its maximum then starts decreasing to reach its minimum then repeat its form again to reach the beginning point of the second cycle and so on. Also we can see that the magnitude of the temperature distribution possess similar variations in the second and third cycles. Moreover, this oscillation decaying as the time t increases. Also, we can see that this oscillation is higher for the diverging tapering than for a non-tapered and converging tapering.

Figs. (12-14) are prepared to see the variation of concentration profile for the coupling parameter N, the degree of anisotropy of the vessel wall n, the contribution of the elastic constraints to the total tethering K, the circumferential Poisson's ratio σ_θ, the initial circumferential viscoelastic stress $T_{\theta o}$ and Brickmann number B_r. It is observed that concentration profile has an opposite behavior as compared to the temperature profile. Fig. (15-a) explain the variation of concentration profile for the Soret number S_r to show the concentration of the fluid decreases as the Soret number S_r increases. Fig. (15-b) represent the variation of concentration of fluid with micopolar parameter m for different values of taper angle ϕ to show that the concentration of fluid decreases rapidly for small values of micropolar parameter m and then take a constant value as m increases.

The wall shear stress and the resistance impedance are important in understanding the development of arterial disease because of the strong correlation between the localization of arteriosclerosis (stenosis) and arterial wall. It is clear that wall shear stress and the resistance impedance distributions profile with the time t have a periodic oscillation form and there are three time cycles where the length of the cycle is equal to 1.6 approximately (see Figs. (16-a) and (16-b)). In the first cycle, the magnitude of the wall shear stress and the resistance impedance distributions start decreasing to reach its minimum then start increasing to reach its maximum then repeat its form again to reach the beginning point of the second cycle and so on. Also we can see that the magnitude of the wall shear stress and the resistance impedance distributions possess similar variations in the second and third cycles. Moreover, this oscillation decaying as the time t increases. Also, we can see that this oscillation is higher for the converging tapering than for a non-tapered and diverging tapering.

Trapping represent an interesting phenomenon for the fluid flow. In the wave frame, streamlines under certain conditions split to trap a bolus which moves as a whole with the speed of the wave. The formation of an internally

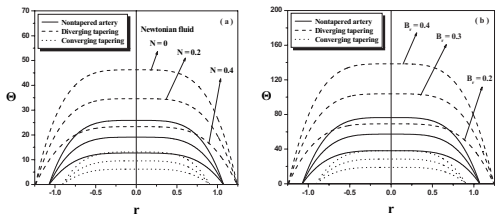

Figure 8 Variation of temperature profiles Θ for N and B_r at t = 0.5, z = 1.5, δ = 0.05, n = 1, K = 10^4, m = 5, σ_θ = 0.5, $T_{\theta o}$ = 0.1 (panels (a) and (b) respectively).

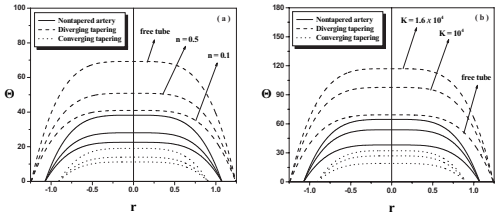

Figure 9 Variation of temperature profiles Θ for n and K at t = 0.5, z = 1.5, δ = 0.05, N = 0.2, m = 5, B_r = 0.2 (panels (a) and (b) respectively).

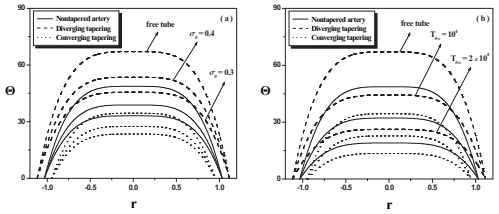

Figure 10 Variation of temperature profiles Θ for σ_θ and $T_{\theta o}$ at t = 0.5, z = 1.5, δ = 0.1, N = 0.2, m = 5, B_r = 0.3 (panels (a) and (b) respectively).

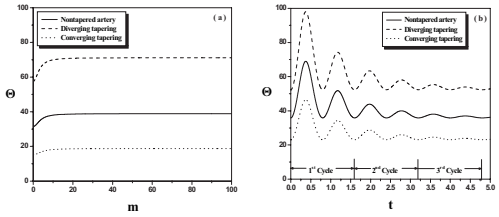

Figure 11 Variation of temperature profiles Θ with micopolar parameter m and the time t for different values of taper angle ϕ (panels (a) and (b) respectively).

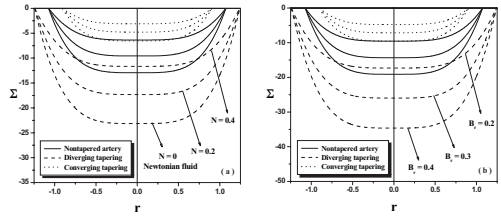

Figure 12 Variation of concentration profiles Σ for N and B_r at t = 0.5, z = 1.5, δ = 0.05, K = 10^4, m = 5, n = 1, $S_r = S_c$ = 0.3, σ_θ = 0.5, $T_{\theta o}$ = 0.1 (panels (a) and (b) respectively).

circulating bolus of the fluid by closed streamline is called trapping phenomena. The bolus defined as a volume of fluid bounded by a closed streamlines in the wave frame is transported at the wave. To study the effect of tethered tube on blood flow, we will vary the previous corresponding parameters, within a physiologically meaningful interval, while keeping all the others fixed in their base values. In choosing the interval of variation for the parameters, we are guided by the following values of these parameters which approximately represent descending aorta of dogs [[1], [24],[29],[31]] as

$$T_{\theta o} = 0.1, \sigma_\theta = 0.51, n = 0.63, K = 1.6x10^4. \qquad (56)$$

The effects of free and tethered tubes on stream lines are illustrated in Fig. (17) to see that the size of the bolus in the free tube smaller than tethered tube. To see the effects of the the taper angle ϕ, the maximum height of stenosis δ on the trapping, we prepared Fig. (18) for various values of the parameters ϕ (= 0, 0.1, -0.1 with t = 0.5, δ = 0.05, n = 1, K = 0, N = 0.2, m = 5) and δ (= 0.05 , 0.07 , 0.09 with t = 0.5, ϕ = 0, n = 1, K = 0, N = 0.2, m = 5). Fig. (18-a) reveals that the size of trapping bolus increases toward the left at $\phi = 0.1$ (diverging tapering artery) and it increases toward the right at $\phi = -0.1$ (converging tapering artery). The effect of the the maximum height of stenosis δ on the trapping is also illustrated in Fig. (18-b), it is observed that there is no separation of flow and the flow is laminar at $\delta = 0.05$ but separation occurs at $\delta = 0.07$ and $\delta = 0.09$. Finally the effect of the coupling number N and the micropolar parameter m on the trapping, we prepared Fig. (19) for various values of the parameters N (= 0, 0.4, 0.8 with t = 0.5, δ = 0.05, n = 1, K = 0, ϕ = 0, m = 5) and m (= 0.001 , 5 , 100 with t = 0.5, δ = 0.005, n = 1, K = 0, ϕ = 0, N = 0.2), it is observed that the trapping is about the center line and the trapped bolus increase in size as the coupling number N increases (the particle size increases) and the inverse occurs such that the volume of the bolus decreases by increasing of micropolar parameter m (micropolar spin parameter).

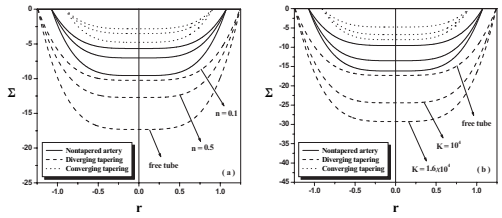

Figure 13 Variation of concentration profiles Σ for n and K at t = 0.5, z = 1.5, δ = 0.1, N = 0.2, m = 5, B_r = 0.2, $S_r = S_c$ = 0.3 (panels (a) and (b) respectively).

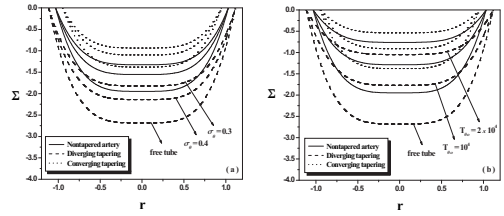

Figure 14 Variation of concentration profiles Σ for σ_θ and $T_{\theta o}$ at t = 0.5, z = 1.5, δ = 0.1, N = 0.2, m = 5, B_r = 0.3, $S_r = S_c$ = 0.2 (panels (a) and (b) respectively).

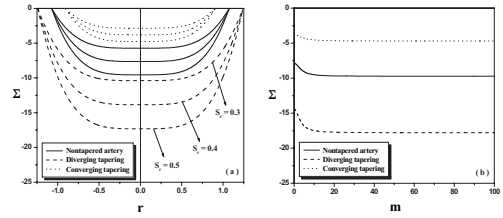

Figure 15 Variation of Σ for S_r (panel (a)) at t = 0.5, z = 1.5, δ = 0.05, N = 0.2, m = 5, n = 1, K = 10^4, B_r = 0.2 and the effect of m on σ (panel (b)).

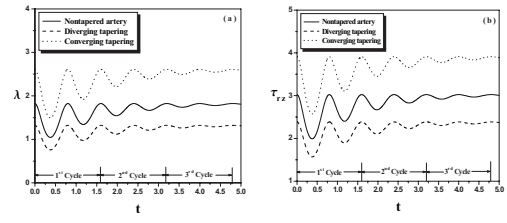

Figure 16 Variation of resistance impedance (resistance to flow) and the wall shear stress distribution τ_{rz} λ with the time t (panels (a) and (b) respectively).

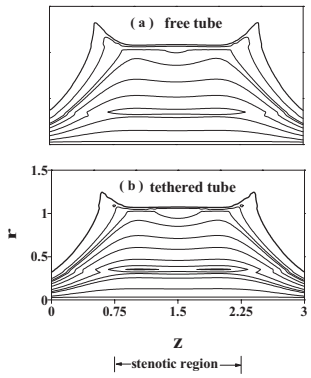

Figure 17 Plot showing streamlines for free and tethered tubes (panels (a) and (b) respectively).

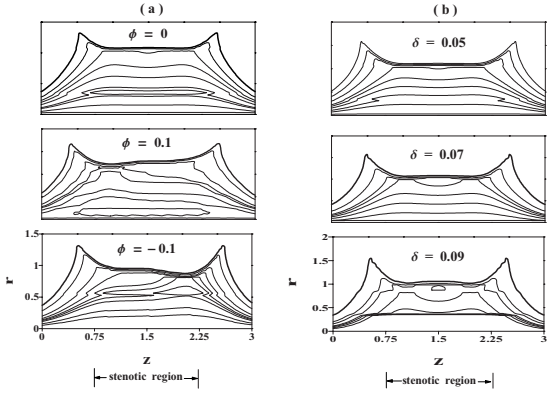

Figure 18 Plot showing streamlines for different values of taper angle ϕ and maximum height of stenosis δ (panels (a) and (b) respectively).

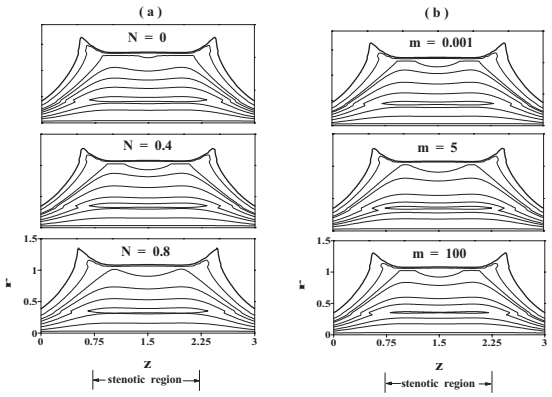

Figure 19 Plot showing streamlines for three different values of coupling number N and micropolar parameter m (panels (a) and (b) respectively).

5. Concluding remarks

The effect of heat and chemical reactions on micropolar fluid model of blood flow through an anisotropically tapered elastic arteries with overlapping stenosis is studied. The exact expressions for stream function, axial velocity, the circumferential microrotation, the temperature and the concentration of fluid are obtained analytically. Graphical results are presented for the wall shear stress distributions and resistance to flow (resistance impedance), axial velocity, the circumferential microrotation, the temperature and the concentration of fluid and trapping. The main finding can be summarized as follows:

• The magnitude of the axial velocity V_z is higher for a Newtonian fluid ($N = 0$) than that for a micropolar fluid these results agree closely with those of Mekheimer and Elkot [13], Srinivasacharya et al. [20] and Devanathan and Parvathamma [25] and the transmission of axial velocity curves through a free tube $(T_{\theta o} = 0, \sigma_\theta = 0.5, n = 1, K = 0)$ is substantially higher than that through the tethered tube.

• The transmission of circumferential microrotation curves through a free tube $(T_{\theta o} = 0, \sigma_\theta = 0.5, n = 1, K = 0)$ is substantially higher than that through the tethered tube in the half region but in the other half it is in the opposite direction.

• The temperature profile increase rapidly for small values of micropolar parameter m (micropolar spin parameter) and then take a constant value as m increases these results agree closely with those of Ikbal et al. [10] while the concentration profile has an opposite behavior as compared to the temperature profile.

• The effect of vessel tapering is an important factor considered in this paper. The results considered three different taper angles of artery which are the converging tapering $\phi < 0$, non-tapered $\phi = 0$ and the diverging tapering $\phi > 0$ in the presence of overlapping stenosis. Under stenotic conditions, the curves through the converging tapered artery $\phi = -0.1\ (< 0)$ are higher than those in the non-tapered artery $\phi = 0$ and the diverging tapered artery $\phi = 0.1\ (> 0)$.

• The wall shear stress and resistance impedance profiles have an oscillation form through the tapered overlapping stenosed arteries and this oscillation decaying as the time increases. Also, we can see that this oscillation is higher for the converging tapering than for a non-tapered and diverging tapering.

• The size of trapped bolus for the stream lines in the free isotropic tube is smaller than those in the tethered tube.

• The size of trapping bolus increases toward the left at diverging tapering artery and it increases toward the right at converging tapering artery.

• In the overlapping stenotic region, by increasing the maximum height of the stenosis δ, the stream lines separate and trapping bolus appear.

• The rapping bolus increase in size as the coupling number N increases (the particle size increases) and the inverse occurs such that the volume of the bolus decreases by increasing of micropolar parameter m (micropolar spin parameter).

Acknowledgement

The authors would like to thank to Prof. M. Abdel-Aty, Editor-in-Chief Applied Mathematics Information Sciences for his invaluable suggestions that lead to the improvement of this paper and to Appl. Math Inf. Sci. journal also Natural Sciences publishing Corporation. The author is grateful to the anonymous referee for a careful checking of the details and for helpful comments that improved this paper.

References

[1] S. Chakravarty and A. Ghosh Chowdhury, Rheol Acta **27**, 418 (1988).
[2] A. C. Eringen, J. math. mech. **16**, 1 (1966).
[3] A. Bharali and A. K. Borkakati, App. Sci. Research **39**, 155 (1982).
[4] A. Ogulua and T.M. Abbeyb, International Communications in Heat and Mass Transfer **32**, 983 (2005).
[5] B. Tashtoush and A. Magableh, Heat Mass Transfer **44**, 297 (2008).
[6] R. Chiba, M. Izumi and Y. Sugano, Arch. Appl. Mech. **78**, 61 (2008).
[7] T. Hayat, M. Umar Qureshi and Q. Hussain, Applied Mathematical Modelling **33**, 1862 (2009).
[8] Sarifuddin, S. Chakravarty and P.K. Mandal, International Journal of Heat and Mass Transfer **52**, 5719 (2009).
[9] Sarifuddin, S. Chakravarty, P. K. Mandal and H. I. Andersson, ZAMP **60**, 299 (2009).
[10] A. Ikbal, S. Chakravarty, Sarifuddin and P.K. Mandal, International Journal for Numerical Methods in Fluids, published online 6 OCT DOI: 10.1002/fld.2438 (2010).
[11] Kh. Mekheimer and M. A. Elkot, Int. J. Pure and App. Math. **4**, 393 (2007).
[12] Kh. Mekheimer and M. A. Elkot, App. Math. Mech. Engl. Ed. **29(8)**, 1093 (2008).
[13] Kh. Mekheimer and M. A. Elkot, Acta Mech Sin **24**, 637 (2008).
[14] Kh. Mekheimer and M. A. Elkot, Chem. Eng. Comm. **197**, 1 (2010).
[15] S. Chakravarty and P.K. Mandal, Mathematical and Computer Modelling **24**, 43 (1996).
[16] S. Chakravarty and P.K. Mandal, International Journal of Non-Linear Mechanics **35**, 779 (2000).
[17] Z. Ismail., I. Abdullah, N. Mustapha and N. Amin, App. Math. and Comp. **195**, 669 (2008).
[18] Kh. S. Mekheimer, Mohammed H. Haroun and M. A. ElKot, Can. J. Phys. **89**, 201 (2011).
[19] P. K. Mandal, International Journal of Non-Linear Mechanics **40**, 151 (2005).
[20] D. Srinivasacharya, M. Mishra and A. R. Rao, Acta Mech. **161**, 165 (2003).
[21] A. Bejan, Convection heat transfer, (2nd Ed.,John Wiley, New York, 1995).

[22] S. Chakravarty, A. Datta and P. K. Mandal, Int. J. Engng Sci. **33**, 1821 (1995).
[23] S. Chakravarty, Rheol Acta **26**, 200 (1987).
[24] H. B. Atabek and H. S. Lew, Biophysical Journal **6**, 481 (1966).
[25] R. Devanathan, S. Parvathamma, Medical and Biological Engineering and Computing **21**, 438 (1983).
[26] D. F. Young, J. Eng. Ind. **90**, 248 (1968).
[27] I. Mirsky, Wave propagation in a viscous fluid contained in an orthotropic elastic tube. Biophysical Journal **7**: 165 (1967).
[28] P. Kalita and R. Schaefer, Arch Comput. Methods Eng. **15**, 1 (2008).
[29] J. R. Womersley, Wright Air Development Center Technical Report TR , 56 (Wright-Patterson AFB, Ohio.1957).
[30] P. Kalita and R. Schaefer, Arch Comput. Methods Eng. **15**, 1 (2008).
[31] H. B. Atabek , Biophysical Journal **8**, 626 (1968).
[32] A.P. Dwivedi, T.S. Pal, L. Rakesh, Indian J. Technol **20**, 295 (1982).
[33] P. Chaturani, R. Pralhad, Biorheology **22**, 303 (1985).
[34] T.V. How, R.A. Black, Biorheology **24**, 337 (1987).

K. S. Mekheimer is presently employed as a professor of applied mathematics in Department of Mathematics, Faculty of Science, Al-Azhar University, Egypt. He obtained his Ph. D. in applied mathematics in 1994 from Al-Azhar University Egypt . He is interested in the field of bio-fluid Mechanics, He has been awarded by the Egyptian Mathematical Society the Prof. Baha El Dien Helmi Ismail Prize , for Supervised on the Best Ph.D. Thesis 2008, Egypt. Also, for the best scientific published research from King Abdu El Aziz University ,K.S.A. , 2010. His Citation overview (22 Dec. 2011) is : 509 and h index: 11. He has been an invited speaker of number of conferences and has published more than 45 research articles in reputed international journals of mathematical and engineering sciences.

M. H. Haroun is presently employed as associate professor of applied mathematics in Department of Mathematics, Faculty of Education, Ain Shams University, Egypt. He obtained his Ph. D. in applied mathematics in 2002 from Ain Shams University , Egypt . He is interested in the field of bio-fluid mechanics. He has been an invited speaker of number of conferences and has published more than 12 research articles in reputed international journals of mathematical and engineering sciences.

M. A. El Kot is presently employed as associate lecture of applied mathematics in Department of Mathematics, Faculty of Science, Suez Canal University, Suez, Egypt. He obtained his master degree of science (M. SC.) in applied mathematics in 2007 from Faculty of science (Ismailia)-Suez canal university, Egypt. Now, he prepare his thesis to obtain (Ph.D.) in applied mathematics. He is interested in the field of bio-fluid mechanics. He has been an invited speaker of number of conferences and has published more than 8 research articles in reputed international journals of mathematical and engineering sciences.